

On the optical extinction and distance of GRS 1915+105

C. Chapuis^{1,2} and S. Corbel^{1,3}

¹ Service d'Astrophysique, DAPNIA bâtiment 709, l'Orme des merisiers, CEA Saclay, F-91191 Gif sur Yvette cedex

e-mail: cchapuis@cea.fr

² Département de physique, bâtiment Buffon,
Université de Versailles, 45 avenue des Etats Unis
F-78035 Versailles cedex

³ Université Paris VII, 2 place Jussieu, F-75251 Paris cedex 05

Submitted: 27 june 2003 Received ; accepted 21 october 2003

Abstract. Based on new millimeter and radio observations, we reevaluate the total hydrogen column density along the line of sight to the microquasar GRS 1915+105 to $N_H = (3.5 \pm 0.3) \times 10^{22} \text{ cm}^{-2}$. Our value is consistent with the one derived from X-ray measurements, namely $(3.8 \pm 0.3) \times 10^{22} \text{ cm}^{-2}$ (Ebisawa et al. 1998). Using the empirical law between the visual extinction and the total column density of hydrogen, A_v is found to 19.6 ± 1.7 mag. This result is ~ 7 mag lower than previously thought, and therefore, a reevaluation of infrared fluxes after dereddening is needed. The revisited kinematic study allows to give a lower limit to the distance of GRS 1915+105, namely 6.0 kpc. Taking into account the most accurate upper limit of distance inferred from radio data (11.2 ± 0.8 kpc; Fender et al. 1999) as well as this lower limit, this implies a distance of 9.0 ± 3.0 kpc.

Key words. Stars: individual: GRS 1915+105 – X-ray: binaries – ISM: extinction – Molecular data

1. GRS 1915+105 and its optical extinction

GRS 1915+105 is a Galactic X-ray binary in the Aquila constellation ($l=45.37^\circ$, $b=-0.22^\circ$), discovered on 15 august 1992 by the WATCH all-sky X-ray monitor on board the GRANAT satellite (Castro-Tirado et al. 1994).

Based on follow-up observations with the VLA, GRS 1915+105 was shown to be the first Galactic source with apparent superluminal motion (Mirabel & Rodríguez 1994). Using the proper motion properties of relativistic radio ejecta observed with MERLIN and under the assumption of a symmetric ejection, the more constraining upper limit of the distance was found to 11.2 ± 0.8 kpc (Fender et al. 1999).

CO absorption lines in the infrared spectrum clearly identified the donor as a K-M III star (Greiner et al. 2001a,2001b). Due to the relative motion of the companion star around the center of mass of the system, these lines were modulated by Doppler effect. The period of the system (33.5 day) and its mass function ($9.5 \pm 3.0 M_\odot$) were obtained. The mass of the compact object was measured to $14 \pm 4 M_\odot$, which unambiguously identify the compact object as a black hole (Greiner et al. 2001b).

During a monitoring observation of GRS 1915+105 by the Ryle telescope at 15 GHz, quasi-periodic oscillations were found and associated with the soft-X-ray variations on the same time-scale (Pooley & Fender 1997). Fast infrared oscillations on time-scales of less than an hour as well as radio oscillations were interpreted as small synchrotron emitting ejections of material (Fender et al. 1997). Then, X-ray dips on time-scales of minutes have been interpreted as the rapid disappearance and refill of the inner accretion disk (Belloni et al. 1997a,1997b). Simultaneous observations revealed ejection of relativistic plasma clouds in the form of synchrotron flares at radio and infrared wavelengths (Mirabel et al. 1998).

There is currently a strong indication that the infrared emission is related to the jet, although it cannot be ruled out that a significant fraction of the infrared flux could be attributed to the disk (Fender et al. 1997). Thus, the infrared magnitudes must be dereddened properly in order to rely the observations to an emission process. For that purpose, the distance and the optical extinction A_v should be measured and their limiting uncertainties carefully calculated.

The optical extinction A_v to the system is the main parameter used to deredden the optical and infrared fluxes. Based on a measurement of the magnitude in the R band,

it was first evaluated to $A_v \sim 30$ mag (Mirabel et al. 1994). This result and the derived $A_K=3.3$ mag (using $\frac{A_v}{A_K}$ from Rieke & Lebofsky 1985) as well, are still used for dereddening (e.g. Fender et al. 1997, Fender & Pooley 2000), although the authors pointed out that these results are uncertain (Fender & Pooley 2000). The position of GRS 1915+105 is known very accurately since the discovery of the radio counterpart (Mirabel et al. 1994). These precise coordinates allowed to perform an HI absorption spectrum during a radio outburst (Rodríguez et al. 1995), as well as a $^{12}\text{CO}(J=1-0)$ spectrum (linked to the column density of molecular hydrogen). A visual extinction of $A_v=26.5 \pm 1$ mag was derived. Meanwhile, another team evaluated the optical extinction to GRS 1915+105 to $A_v=18-24$ mag (Castro-Tirado, Geballe & Lund 1996) with the help of the X-ray hydrogen absorption column density and the pioneering work of Gorenstein (1975) relating the optical extinction to the total hydrogen column density. Moreover, we have to note that the hydrogen column density derived from Si and Fe edges (X-ray observations with Chandra) is substantially higher than $5 \times 10^{22} \text{cm}^{-2}$ (leading to an extinction of 28 mag) and should imply additional local absorption (Lee et al. 2002) although the Mg and S edges lead to consistent values of N_H with the one of Ebisawa et al. (1998). An overestimate of the extinction would allow higher dereddened fluxes in K bands and flat spectrum from radio to IR (Fuchs et al. 2003). Subsequently, the knowledge of the optical extinction of GRS 1915+105 is of prime importance for understanding the nature of the physical processes which are involved in the infrared/optical range. Thus, an accurate estimate of the total extinction toward GRS 1915+105 is needed. In order to understand the origin of these discrepancies, we conducted millimeter observations to estimate the molecular component which represent a significant contribution to the optical extinction.

We describe our observations and method in 2. Our results are reported in 3 and their implications discussed. The conclusions are then summarized in 4.

2. Observations and method

2.1. Observations

2.1.1. IRAM

Using the autocorrelator as a backend connected to a 3 mm SIS receiver, we performed a high resolution $^{12}\text{CO}(J=1-0)$ velocity spectrum ($\sim 0.2 \text{ km.s}^{-1}$) at 115 GHz along the line of sight of GRS 1915+105 (Figure 1) on 1998 June 7 at the 30 m single dish antenna of IRAM (Spain). The half power beamwidth (FWHM) of the telescope at 115.271 GHz was $27.5''$. The main beam efficiency and the forward efficiency were respectively equal to 0.68 and 0.92 while a typical system temperature of $\sim 380\text{K}$ was observed.

The calibrated spectrum (Figure 1) was fitted with Gaussians to evaluate the central LSR velocity. The areas were measured by summing the antenna temperature

for each channel associated to a molecular cloud. We gave names to clouds which were simply constructed by beginning it with an MC (like molecular cloud) and ending it with the rough fitted LSR velocity in km s^{-1} . The characteristics of the clouds are reported in Table 1.

2.1.2. SEST

We conducted millimeter observations with the 15 m Swedish-ESO Submillimeter Telescope (SEST) located at La Silla (Chile) on 1999 March 2. Spectra were obtained along the line of sight of GRS 1915+105 ($^{13}\text{CO}(1-0)$ line). The FWHM beamwidth of the SEST is $45''$ at 115.27 GHz and the main beam efficiency is 0.70 at this frequency. After checking that the OFF position ($\alpha(2000) = 19^{\text{h}}07^{\text{m}}59.37^{\text{s}}$ $\delta(2000) = 11^{\circ}08'27.1''$) was free of emission, we observed in position-switching mode. The backend was an acousto-optical spectrometer (AOS) with a frequency bandwidth of 1 GHz and a velocity resolution of 1.8 km.s^{-1} at 115.27 GHz. The system was calibrated with the chopper wheel method. The system temperature during the observations was $\sim 650 \text{ K}$ at 115.27 GHz for G 45.45+0.06 and 690 K at the same frequency for G 45.12+0.13

Spectra along the line of sight of H II regions close to GRS 1915+105 were also needed to help and resolve the distance ambiguity (see next section). During the same run, we therefore performed $^{12}\text{CO}(J=1-0)$ spectra along the line of sight of two H II regions: G 45.45+0.06 and G 45.12+0.13 (Figure 2).

2.2. Method

We assumed that the Galaxy rotates in a purely circular motion and determined the close and far distances using $R_0 = 8.5 \text{ kpc}$ and $\Theta_0 = 220 \text{ km s}^{-1}$ as standard rotation constants (R_0 , galactocentric distance of the Sun and Θ_0 , circular velocity of the Sun), using the rotation curve of Fich et al. (1989).

Our aim was to collect a maximum of information along the line of sight of H II regions close to GRS 1915+105 as well as for GRS 1915+105 itself. We gathered HI informations, CO spectra and absorption lines in order to help and locate the clouds at the most accurate distances.

This method was already used to evaluate the first distance to a soft gamma repeater, i.e. SGR 1806-20 (Corbel et al. 1997, Corbel & Eikenberry 2003) and repeated later after the discovery of a new soft gamma repeater, i.e. SGR 1627-41 (Corbel et al. 1999).

In order to convert the results from observations such as the column density of atomic hydrogen and the integrated antenna temperature of a molecular cloud in the $^{12}\text{CO}(J=1-0)$ line into a total hydrogen column density and then to the optical extinction A_v , we proceed as follows.

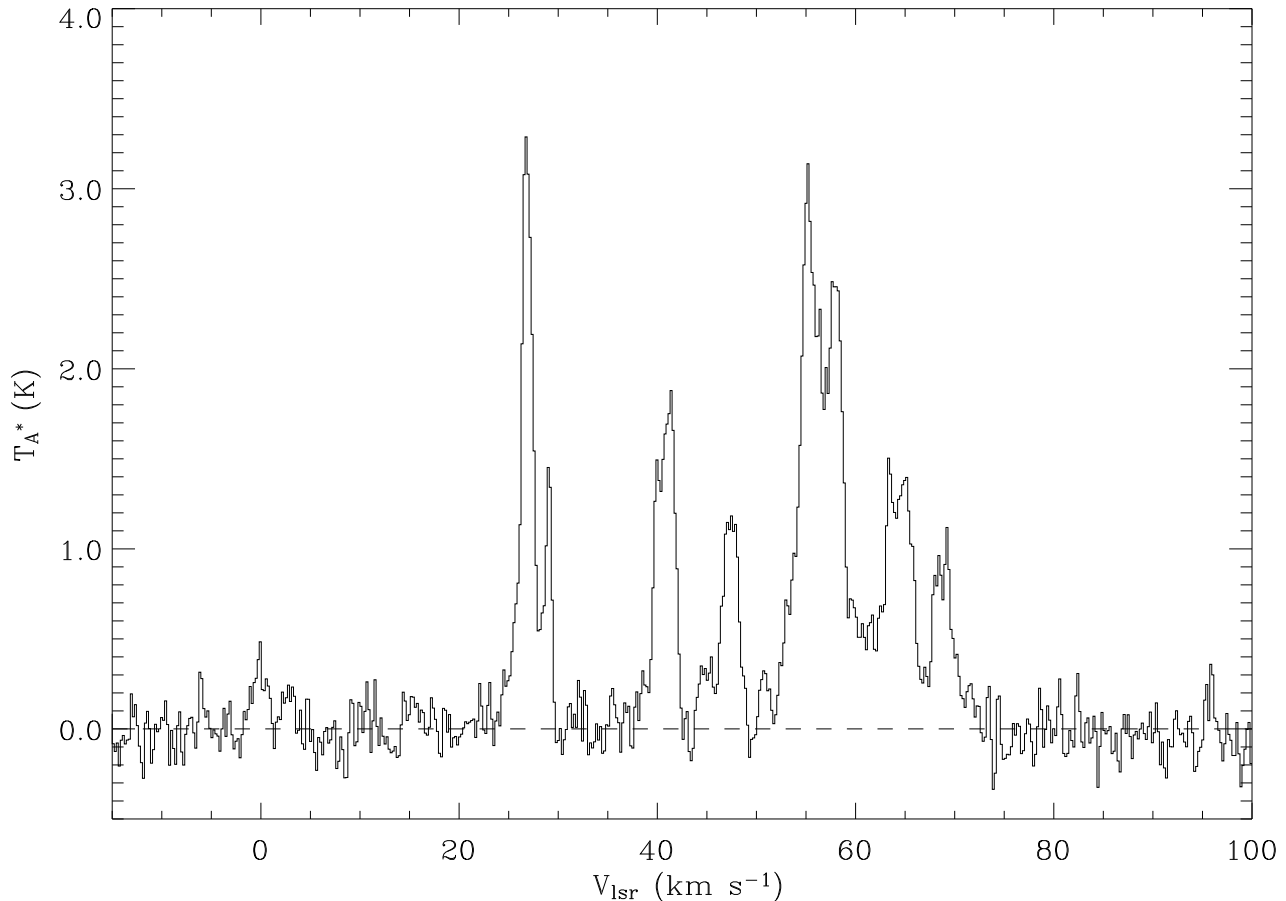


Fig. 1. $^{12}\text{CO}(J=1-0)$ antenna temperature spectrum along the line of sight of GRS 1915+105 performed at IRAM

(i) Evaluation of the integrated antenna temperature $\int T_A^* dv$ in the $^{12}\text{CO}(J=1-0)$ line for each molecular cloud in the spectrum of GRS 1915+105 .

(ii) Converting this area into the integrated main beam temperature $W_{CO} = \int T_{mb} dv$. This conversion was done by dividing $\int T_A^* dv$ by 0.74, which is the conversion factor for IRAM. Indeed, according to the user manual of IRAM, the relation between the main beam brightness temperature T_{mb} and the antenna temperature T_A^* is $T_{mb} = \frac{F_{eff}}{B_{eff}} T_A^*$, with $F_{eff}=0.92$ and $B_{eff}=0.68$ the forward efficiency and the beam efficiency respectively.

(iii) The X_{CO} factor is defined as the fraction between the column density of molecular hydrogen to the integrated area of the main beam temperature and can be written as follows:

$$X_{CO} = \frac{N_{H_2}}{W_{CO}}$$

We adopted the value of the X_{CO} factor (Strong and Mattox 1996):

$$X_{CO} = \frac{N_{H_2}}{W_{CO}} = (1.9 \pm 0.2) \times 10^{20} \text{ K}^{-1} \text{ km}^{-1} \text{ s cm}^{-2}$$

This value was obtained by comparing $^{12}\text{CO}(J=1-0)$ intensity and gamma-ray/EGRET observations.

Why adopting this particular value of the X_{CO} ? Four different methods (Dickman 1975, Thaddeus & Dame 1984, Bloemen et al. 1986, Solomon et al. 1987) have led to similar and consistent values (Solomon & Barrett 1991). Moreover, the analysis of the gamma-ray data from the *COS-B* observatory lead to a value of $2 \times 10^{20} \text{ K}^{-1} \text{ km}^{-1} \text{ s cm}^{-2}$ for the X_{CO} factor (Bertsch et al. 1993). The most recent data for the Galactic diffuse gamma-ray emission are from *EGRET* onboard the *Compton Gamma-Ray Observatory*, which is more sensitive and also has a much higher spatial resolution. Our adopted value of X_{CO} ($(1.9 \pm 0.2) \times 10^{20} \text{ K}^{-1} \text{ km}^{-1} \text{ s cm}^{-2}$; Strong & Mattox 1996) has been derived using the *EGRET* data. This result is consistent with measurement at high galactic latitudes ($1.8 \times 10^{20} \text{ K}^{-1} \text{ km}^{-1} \text{ s cm}^{-2}$; Dame et al. 2001). Nevertheless, with the help of another method and the same *EGRET* data set, a lower X_{CO} - $1.6 \times 10^{20} \text{ K}^{-1} \text{ km}^{-1} \text{ s cm}^{-2}$ - was found, which is still consistent with a value of $\sim 2 \times 10^{20} \text{ K}^{-1} \text{ km}^{-1} \text{ s cm}^{-2}$ (Hunter et al. 1997). Also, one might wonder about the influence of metallicity, cosmic ray density and the UV radiation field on the evaluation of the X_{CO} factor. Indeed, a decrease of the X_{CO} factor could be re-

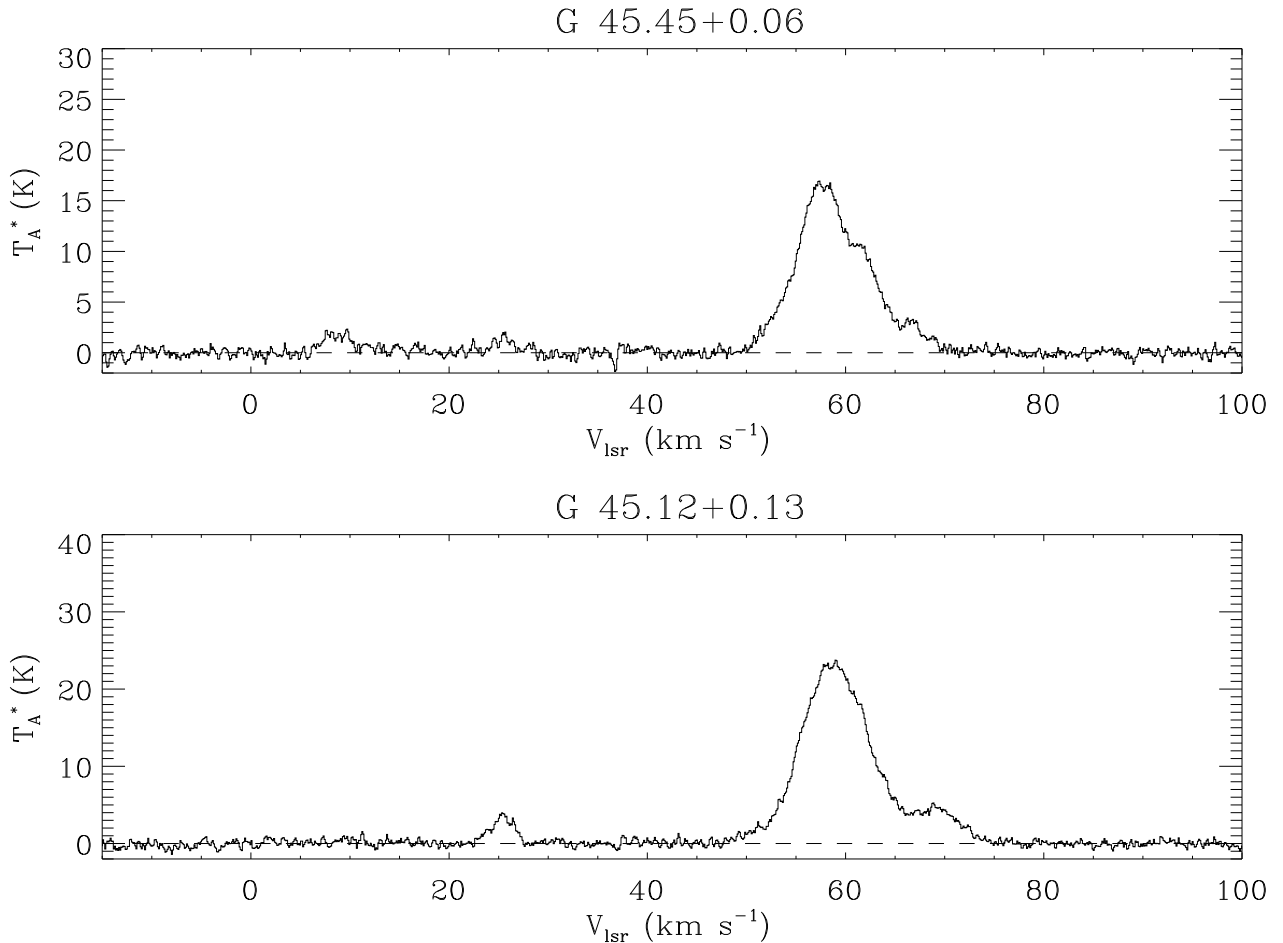


Fig. 2. a $^{12}\text{CO}(J=1-0)$ antenna temperature spectrum along the line of sight of the H II region G 45.45+0.06 performed with HRS/SEST on 2 march 1999 b. same comments for G 45.12+0.13

lated to a higher metallicity (Arimoto, Sofue & Tsujimoto 1996; Pilyugin 2001; Boselli, Lequeux & Gavazzi 2002). Furthermore, there are evidences of radial variations of X_{CO} (Arimoto, Sofue & Tsujimoto 1996). At the longitude of GRS 1915+105, the galactocentric radii of the molecular clouds on the line of sight lies in the range of 6 to 8.5 kpc (using the rotation curve of Fich et al. 1989). Therefore, if there are radial variations of X_{CO} , then the expected variation of X_{CO} would be low for the line of sight to GRS 1915+105. Moreover, in this range of galactic radii, the oxygen abundance ($12 + \log(\text{O}/\text{H}) = 8.9$; Arimoto, Sofue & Tsujimoto 1996), allows $X_{\text{CO}} = 1.95 \times 10^{20} \text{ K}^{-1} \text{ km}^{-1} \text{ s cm}^{-2}$, according to the empirical law, $\log X_{\text{CO}} = -1.01 \times (12 + \log(\text{O}/\text{H})) + 29.28$ (Boselli, Lequeux & Gavazzi 2002). At galactocentric distance of 6 to 8.5 kpc, we are very far from the central region of the Galaxy and their potential problems (Paglione et al. 2001). Furthermore, our adopted value is the mean of the interval including on one hand, the not-so “standard” value $2.3 \times 10^{20} \text{ K}^{-1} \text{ km}^{-1} \text{ s cm}^{-2}$ (Strong et al. 1988) and, on the other hand, the accurate value from EGRET data set to $1.6 \times 10^{20} \text{ K}^{-1} \text{ km}^{-1} \text{ s cm}^{-2}$ (Hunter et al.

1997). At last, we share Solomon & Barrett 1991 point of view : “CO to H_2 conversion factor is fairly robust - robust but not perfect”.

Chaty et al. (1996) used $X_{\text{CO}} = 3.6 \times 10^{20} \text{ K}^{-1} \text{ km}^{-1} \text{ s cm}^{-2}$ (Sanders, Solomon & Scoville 1984) and T_A^* instead of T_{mb} . We calculated the integrated antenna temperature in the $^{12}\text{CO}(J=1-0)$ line for each molecular cloud for which we considered 25 percent uncertainty of the estimated value. These results are summarized in table 1.

(iv) Inferred from a HI absorption spectrum of GRS 1915+105 during an outburst, we used the total atomic hydrogen column density $N_{\text{HI}} = 1.73 \times 10^{22} \frac{T_s}{100\text{K}} \text{ cm}^{-2}$ (Rodríguez et al. 1995), where T_s is the spin temperature. The total column density of hydrogen should then be evaluated, taking into account the atomic and molecular components by the calculation

$$N_{\text{H}} = N_{\text{HI}} + 2 N_{\text{H}_2}$$

(v) Predehl & Schmitt (1995) reevaluated the proportionality factor relying empirically the visual extinction and the total column density of hydrogen to $\frac{N_{\text{H}}}{A_v} = 1.79$

$10^{21} \text{ cm}^2 \text{ mag}^{-1}$ after the pionnering work of Gorenstein (1975). The optical extinction should then be derived from the total column density of hydrogen by the simple relation.

$$A_v = \frac{N_H}{1.79 \cdot 10^{21}} \text{ mag}$$

3. Results

3.1. Extinction along the line of sight of GRS 1915+105

Our first goal is to calculate the maximum value of the total column density of hydrogen. For that purpose, we need to use all the available atomic and molecular matter along the line of sight of GRS 1915+105. Following the procedure described in the previous section, the results of our observations, i.e. velocity, distance, integrated antenna temperature and N_{H_2} of each cloud, are summarized in table 1. We calculated the total column density of molecular hydrogen

$$N_{H_2} = (8.8 \pm 1.4) \times 10^{21} \text{ cm}^{-2}$$

The value of Chaty et al. (1996) would be consistent with this one, using the same X_{CO} .

The total column density of hydrogen becomes

$$N_H = (3.5 \pm 0.3) \times 10^{22} \text{ cm}^{-2}$$

taking into account the HI column density value of (Rodríguez et al. 1995). This value is consistent with the one of Ebisawa et al. (1998) derived from ASCA X-ray observations of GRS 1915+105, which is the most accurate to date: $N_H = (3.8 \pm 0.3) \times 10^{22} \text{ cm}^{-2}$. Subsequently, it is not necessary to locate each cloud accurately, since all the absorbing matter lies between the system and us. Any possible additional absorption seen in the X-ray spectra should then have a local origin. According to the proportionality factor relying empirically the visual extinction and the total column density of hydrogen (Predehl & Schmitt 1995), we finally found

$$A_v = 19.6 \pm 1.7 \text{ mag.}$$

This estimate is ~ 7 mag lower than 26.5 (Chaty et al. 1996), which was based on an overevaluated X_{CO} by a factor of ~ 2 . The visual extinction is still consistent with the high observed reddening of the source in the infrared and consistent with the suggested value of ~ 20 mag (Mahoney et al. 1997) and with the interval 18-24 calculated earlier (Castro-Tirado, Geballe & Lund 1996). Our value implies that the previous dereddening of infrared data processed with A_v from 26.5 to 30 are uncorrect.

We note that a possible negligible excess around 2 km.s^{-1} can be seen on Figure 1, which effects are negligible on N_{H_2} and therefore on A_v . Its velocity, confirmed by a HI difference spectrum (Dhawan et al. 2000), would suggest either a solar component or a close to GRS 1915+105 component.

3.2. Is it possible to constrain the distance to GRS 1915+105 ?

Using the rotation curve of the Galaxy (Fich et al. 1989) and the observed $^{12}\text{CO}(J=1-0)$ luminosities, we estimate the far and near kinematic distances of each molecular cloud. These values are reported into the table 1 for the line of sight of GRS 1915+105 (Figure 1). Since all the available atomic and molecular matter is taken into account and is consistent with the value derived from X-ray observations (i.e., $N_H = (3.8 \pm 0.3) \times 10^{22} \text{ cm}^{-2}$, Ebisawa et al. 1998), it is not necessary to locate the molecular cloud accurately along the line of sight in order to discuss whether GRS 1915+105 is closer or beyond each of them. We just have to identify the farthest cloud and to evaluate its kinematic distance accurately. This would then be the lower limit of the distance to GRS 1915+105.

G 45.45+0.06 and G 45.12+0.13 are two H II regions, respectively 18 arcmin and 26 arcmin away from GRS 1915+105. The spectrum of G 45.45+0.06 reveals molecular clouds around 10, 25 km.s^{-1} and a complex between 50 to 70 km.s^{-1} as well (Figure 2) - FWHM $\sim 10 \text{ km s}^{-1}$ -. This large complex - [46,49] - was still reported as associated to four H II regions (Dame et al. 1986). Among them, the two H II regions close to GRS 1915+105 are noted in the map Fig.5 of Dame et al. (1986). The FWHM distribution spreading for the largest galactic molecular clouds lies typically in the range 4-15 km s^{-1} and peaks around 10 km s^{-1} . Along the line of sight of GRS 1915+105, MC27 is at the near distance (Dame et al. 1986), cf. table 1. Surprisingly, no molecular matter is seen close to the 41 km.s^{-1} velocity in both spectra of G 45.45+0.06 and G 45.12+0.13 (Figure 2) although the line of sight to GRS 1915+105 exhibits additionnal HI absorption at $41 \pm 6 \text{ km.s}^{-1}$ relative to the line of sight to G 45.45+0.06 (Rodríguez et al. 1995). It was therefore claimed that the additionnal HI absorption was farther than G 45.45+0.06 (Rodríguez et al. 1995), so that GRS 1915+105 was beyond G 45.45+0.06 and then behind a cloud located at the kinematic distance of $9.4 \pm 0.5 \text{ kpc}$, which we consistently located at 9.1 kpc (cf. table 1). This is no longer an evidence if we assume, as Rodríguez et al. (1995) did, that the CO feature and the HI additional absorption onto GRS 1915+105 come from the same cloud, i.e. MC41. We suggest that the complex along the line of sight of GRS 1915+105, for which velocities are seen from 50 to 70 km.s^{-1} , is an extension of the one seen along both lines of sight of the two H II regions (Figure 2). Thus, its location should be the tangent point. It has a large contribution to the extinction to GRS 1915+105 ($\sim 6 \text{ mag}$), so that it could not be possible to explain the A_v without its contribution. This is confirmed by HI observations which allowed to put a lower distance to GRS 1915+105 beyond the tangent point (Rodríguez et al. 1995). GRS 1915+105 is then behind this complex and therefore, the closest lower limit is the distance to the tangent point, i.e., the distance to this complex, namely 6.0 kpc.

Name	LSR	$W(CO)^* = \int T_A^* dv$	N_{H_2}	$\sigma_{N_{H_2}}$	A_v	near distance	far distance	MC estimated distance
	km.s ⁻¹	K.km.s ⁻¹	cm ⁻²	cm ⁻²	mag	kpc	kpc	kpc
GRS 1915+105								
MC27	26.8	4.92	1.26	0.34	1.41	1.8	10.1	1.8
MC29	29.0	1.39	0.36	0.098	0.40	2.0	9.9	2.0
MC41	40.8	4.25	1.09	0.30	1.22	2.9	9.1	
MC47	47.4	2.50	0.64	0.17	0.72	3.4	8.6	
MC56	56.4	13.9	3.57	0.97	3.99	4.2	7.7	
MC64	64.3	5.10	1.31	0.36	1.46	5.4	6.6	
MC69	68.9	2.20	0.56	0.15	0.63	6.0	6.0	6.0
total		34.3	8.79	1.4	9.83			

Table 1. Summary of molecular clouds observations from $^{12}\text{CO}(J=1-0)$ spectra with IRAM and SEST for GRS 1915+105 line of sight, where the columns represent (1) name, (2) LSR fitted velocity in km s⁻¹ (3) area of the antenna temperature T_A^* in K km s⁻¹ (4) N_{H_2} in 10²¹ cm⁻² (5) $\sigma_{N_{H_2}}$ in 10²¹ cm⁻² (6) optical extinction A_v in magnitude (7)(8)(9) columns meaning is explicit

Due to their non negligible contributions to the extinction (cf table 1), MC41 and MC47 have to be taken into account in order to describe the extinction properly. We point out that the optical extinction should be 2 mag lower (i.e. 17.5 mag) if MC41 and MC47 are behind GRS 1915+105. The implied hydrogen column density ($3.1 \times 10^{22} \text{cm}^{-2}$) is still consistent with the most accurate X-ray measurement in a two sigma confidence level (Ebisawa et al. 1998), although it is at the far end of the interval and that it could mean that we need at least the contribution of one or both MC41 and MC47 to be consistent with measurements with a higher confidence level.

During 1997 October/November, multiple relativistic ejections from GRS 1915+105 were observed in radio range with MERLIN and an upper limit of the distance to GRS 1915+105 was deduced to 11.2 ± 0.8 kpc (Fender et al. 1999), which is about 1 kpc lower than the upper pionnering value of Mirabel & Rodríguez (1994) inferred from a similar discussion. This upper limit is consistent with Hi emission spectra in this direction of the sky (Radhakrishnan et al. 1972) because of a lack of absorption at negative LSR radial velocities (Rodríguez et al. 1995, Dhawan, Goss & Rodriguez 2000).

Thus, the distance of GRS 1915+105 should be greater than 6.0 and less than 12.0 kpc, using a one sigma allowed interval on the upper limit of Fender et al. (1999). We then put GRS 1915+105 at 9.0 ± 3.0 kpc. Note carefully that the 3 kpc interval is not a one sigma confidence level. We consider this expression as an interval and not as an evaluation of the distance at a one sigma significance. The consequence of that result, enforced by the lower A_v we found, is that GRS 1915+105 is less luminous than expected in the optical and infrared ranges.

3.3. A metal rich local dust absorption?

Assuming solar abundances, Chandra spectral observation led to an H column density derived from silicon and iron K-edges ($(8.4_{-0.2}^{+0.1}) \times 10^{22} \text{cm}^{-2}$ and $(9.3_{-1.3}^{+1.6}) \times 10^{22} \text{cm}^{-2}$ respectively) substantially higher than the values derived from sulphur and magnesium K-edges ($(3.2_{-0.6}^{+0.1}) \times 10^{22} \text{cm}^{-2}$ and $(3.1_{-0.3}^{+0.3}) \times 10^{22} \text{cm}^{-2}$ respectively)(Lee et al. 2002). The last two values are both consistent with our calculated N_H as well as the one from ASCA (Ebisawa et al. 1998). Based on the values of N_H inferred from Si and Fe edges, it was suggested that either a highly unusual supernova or external supernova activity local to the binary could explain the overabundance in iron and silicon (Lee et al. 2002). Indeed, it seems that a 10^{52} erg kinetic energy SNe with high mixing, helped by a small mass cut and/or asphericity in explosion can provide high amounts of ejected ^{56}Ni , and thus ejected iron after ^{56}Ni decay (Nomoto et al. 2003). Could this metal rich component be a relic of the SNR now diluted in the ISM?

We would like to note several alternative explanations since such values of the N_H are inconsistent with our measurement of the total content along the line of sight. We propose that a Si/Fe enriched component should be either along the line of sight or local to GRS 1915+105. The matter could come from a bright star (ISOGAL-PJ191511.2+105622) seen in the ISOGAL survey (Felli et al. 2000), 18" away to the line of sight of GRS 1915+105 and classified as an AGB star (Fuchs et al. 2003) after a dereddening with $A_v=20$ mag. Although the photosphere is thought to be originally solar in composition, some extremely metal poor post AGB stars (A to F stars) are depleted in elements such as Fe, Ca, Si, Cr (two orders of

magnitude below solar) and with solar photospheric abundances of C, N, O, S and Zn (Mathis & Lamers 1992). The missing elements should be incorporated into grains that were separated from atmosphere. If this AGB is at the same distance than GRS 1915+105, only little material can account to the anomalous abundances of Si/Fe (Fuchs et al. 2003). On the other hand, if this AGB star is much closer to the Earth than GRS 1915+105, its surrounding nebula could likely have contaminate the line of sight of GRS 1915+105 and enriched it in heavy elements. Using the Draine extinction law (1989) and the same $A_v=20$ mag as for GRS 1915+105, the ISOGAL-PJ191511.2+105622 spectrum exhibits a bump at $9.7\mu\text{m}$. Therefore, the extinction to ISOGAL-PJ191511.2+105622 would be overestimated, and then the distance closer. In order to give some solidity to this hypothesis, using the rough value of 10 mag, the bump disappears in the spectrum which becomes more likely the one of a star in this range of energy than the previous one (Fuchs, private communication). The derived dereddened $7\mu\text{m}$ and $15\mu\text{m}$ magnitudes are respectively equal to $[7]=7.60$ mag and $[15]=7.04$ mag. The $[15]-[7]-[15]$ diagram (Felli et al. 2000, Figure 1.) reinforces the AGB association. Although the value of ~ 10 mag is a rough estimate of its optical extinction, it implies however that this AGB lies in front of the big complex located at the tangent point, and therefore with an upper limit of its distance of 6.0 kpc. The angular separation between GRS 1915+105 and the line of sight of this AGB is $18''$. At a distance of 6 kpc, this is converted to a projected distance on the plane of the sky of 0.5 pc. Moreover, it is known that an AGB star can eject material on distances as far as 1 pc. We thus claim that the surrounding dust of this AGB type star, closer to the Earth and with a lower extinction than GRS 1915+105, could contaminate significantly the line of sight of GRS 1915+105 and contribute to the anomalous metallicity observed in the X-rays with Chandra (Lee et al. 2002) which cannot be taken into account with our millimeter and radio determinations of N_H and A_v .

4. Conclusions

The column density of hydrogen along the line of sight of GRS 1915+105 is found to $N_H = (3.5 \pm 0.3) \times 10^{22} \text{ cm}^{-2}$. This value is consistent with the X-ray observations of ASCA (Ebisawa et al. 1998) constraining the column density of hydrogen to $(3.8 \pm 0.3) \times 10^{22} \text{ cm}^{-2}$.

The visual extinction inferred from molecular spectra and H α absorption spectrum is $A_v = 19.6 \pm 1.7$ mag, consistent with the guess of Castro-Tirado, Geballe & Lund (1996) who found the likely range of 18-24 mag. Our value of the optical extinction is then still consistent with a high reddening of the source. Based on Cardelli et al. (1989) relations between A_v and A_λ , we deduce A_λ from U to L bands (Table 2). In order to evaluate the uncertainty on A_λ , we took into account the uncertainty on A_v as well as the spreading of the values of Cardelli et al. (1989) as uncertainty on the proportionality factor between A_v and

A_λ . The consequence is that all dereddening using extinctions of $A_K=3.0$ mag or more (Chaty et al. 1996, Fender & Pooley 2000) should be reprocessed and their results reevaluated.

With the help of the rotation galactic rotation description (Fich et al. 1989), the properties of close to GRS 1915+105 H II regions, $^{12}\text{CO}(J=1-0)$ spectra along the line of sight of GRS 1915+105 and two close H II regions as well as the most recent upper limit of distance (Fender et al. 1999), we reevaluated the distance to GRS 1915+105 at 9.0 ± 3.0 kpc. It is important to notice that no molecular cloud is seen at a velocity close to 40 km.s^{-1} in both line of sights of the two close to GRS 1915+105 H II regions, i.e. G 45.45+0.06 and G 45.12+0.13.

Acknowledgements. We acknowledge Y. Fuchs and S. Chaty for valuable discussion. We warmly thank S. Shore for his relevant comments on the paper. We are grateful to S. Leon for conducting the IRAM observations. This research has made use of the SIMBAD database, operated at CDS, Strasbourg, France and of NASA's Astrophysics Data System Abstract Service.

References

- Arimoto, N., Sofue, Y., Tsujimoto, T. 1996, PASJ, 48, 275
- Belloni T., Mendez M., King A.R., van der Klis M., van Paradijs J., 1997a, ApJ, 479, L145
- Belloni T., Mendez M., King A.R., van der Klis M., van Paradijs J., 1997b, ApJ, 488, L109
- Bertsch, D.L. et al. 1993, ApJ, 416, 587
- Bloemen J.B.G.M., Strong A.W., Blitz L., Cohen R.S., Dame T.M., Grabelsky D.A., Hermesen W., Lebrun F. and Thaddeus P., 1986, A&A, 154, 25
- Boselli, A., Lequeux, J., and Gavazzi, G. 2002, *â*, 384, 33
- Cardelli J.A., Clayton G.C., and Mathis J.S., 1989, ApJ, 345, 245
- Castro-Tirado A.J., Brandt A.J., Lund N., Lapshov I., Sunyaev R.A., Shlyapnikov A.A., Guziy S., Pavlenko E.P. 1994, ApJS, 92, 469
- Castro-Tirado A.J., Geballe T.R., Lund N., 1996, ApJ, 461, L99
- Chaty S., Mirabel I.F., Duc P.A., Wink J.E., Rodríguez L.F. 1996, A&A, 310, 825
- Corbel S., Wallyn P., Dame T. M., Durouchoux P., Mahoney W. A., Vilhu O., Grindlay J. E., 1997, ApJ, 478, 624
- Corbel S., Chapuis C., Dame T. M., Durouchoux P., 1999, ApJ, 526, L29
- Corbel, S., Eikenberry, S.S., 2003, A&A, submitted
- Dame T.M., Emelgreen B.G., Cohen R.S., Thaddeus P., 1986, ApJ, 305, 892
- Dame, T.M., Hartmann, D. & Thaddeus, P. 2001, ApJ, 547, 792
- Dhawan, V., Goss, W.M., Rodriguez, L.F. 2000, ApJ, 540, 863
- Dickman, R.L. 1975, ApJ, 202, 50
- Draine, B.T. 1989, in Infrared spectroscopy in astronomy, 93
- Ebisawa K. et al., 1998, "Hot universe" Kluwer Academic, IAU symposium N188, 392
- Felli, M., Comoretto, G., Testi, L., Omont, A., & Schuller, F. 2000, A&A, 362, 199
- Fender R.P, Pooley G.G., Brocksopp C., Newell S.J., 1997, MNRAS, 290, L65

Band	U	B	V	R	I	J	H	K	L
λ (μm)	0.365	0.44	0.55	0.70	0.90	1.25	1.65	2.2	3.6
A_λ (mag)	30.8 \pm 2.8	26.2 \pm 2.3	19.6\pm1.7	14.7 \pm 1.3	9.4 \pm 0.8	5.5 \pm 0.5	3.7 \pm 0.4	2.2 \pm 0.3	1.1 \pm 0.1

Table 2. Summary of GRS 1915+105 extinctions from U to L bands. Lines (1) Band, (2) wavelength λ in μm (3) Value and uncertainty of A_λ for each band in magnitudes

- Fender R.P, Garrington S.T., McKat D.J., Muxlow T.W.B., Pooley G.G., Spencer R.E., Stirling A.M., Waltman E.B., 1999, MNRAS, 304, 865
- Fender, R.P, Pooley 2000, MNRAS, 318, L1
- Fich, M., Blitz, L., Stark, A.A. 1989, ApJ, 342, 272
- Fuchs, Y., Mirabel, I.F., Claret, A. 2003, A&A, 404, 1011
- Gorenstein, P. 1975, ApJ, 198, 95
- Greiner, J., Cuby, J.G., McCaughrean, M.J., Castro-Tirado, A.J., Mennicken, R.E. 2001a, A&A, 373, L37
- Greiner, J., Cuby, J.G., McCaughrean, M.J. 2001b, Nature, 414, 522
- Hunter, S.D. et al. 1997, ApJ, 481, 205
- Lee, J.C., Reynolds, S., Remillard, R., Schultz, N.S., Blackman, E.G., Fabian, A.C. 2002, ApJ, 567, 1102
- Mahoney, W.A. et al. 1997, 4th Compton Symposium, AIP 410, 912
- Mathis, J.S., Lamers, H.J.G.L.M. 1992, A&A, 259, L39
- Mirabel, I.F., Rodríguez, L.F. 1994, Nature, 371, 46
- Mirabel, I.F., Duc, P.A., Rodríguez, L.F., Teyssier, R., Paul, J., Claret, A., Auriere, M., Golombek, D., Martí, J. 1994, A&A, 282, L17
- Mirabel, I.F., Dhawan, V., Chaty, S., Rodríguez, L.F., Martí, J., Robinson, C.R., Swank, J., Treballe, T.R. 1998, A&A, 330, L9
- Nomoto, K., Maeda, K., Umeda, H., Tominaga, N., Ohkubo, T., Deng, J., Mazzali, P.A., 2003, Carnegie observatories astrophysics series, vol. 4: Origin and evolution of the elements, ed. A. McWilliam & M. Rauch, astro-ph/0306412
- Paglione, T.A.D. et al. 2001, ApJS, 135, 183
- Pilyugin, L.S. 2001, A&A, 369, 594
- Pooley G. G., Fender R. P., 1997, MNRAS, 292, 925
- Predehl, P., Schmitt, J.H.M.M., 1995, A&A, 293, 889
- Radhakrishnan, V. Brooks, J.W., Goss, W.M., Murray, J.D., Schwarz, U.J. 1972, ApJS, 24, 1
- Rieke G.H., Lebofsky, M.J., 1985, ApJ, 288, 618
- Rodríguez, L.F., Gérard, E., Mirabel, I.F., Gómez, Y., Velásquez, A., 1995, ApJS, 101, 173
- Sanders, D.B., Solomon, P.M. & Scoville, N.Z. 1984, ApJ, 276, 182
- Solomon, P.M., Rivolo, A.R., Barrett, J.W. & Yahil, A. 1987, ApJ, 319, 730
- Solomon, P.M. & Barrett, J.W. 1991, Proceedings of the 146th IAU symposium, 235
- Strong, A.W., Bloemen, J., Dame, T. et al. 1988, A&A, 207, 1
- Strong, A. W. & Mattox, J. R. 1996 A&A, 308, L21
- Thaddeus, P. & Dame, T.M. 1984, Workshop on star formation, in reports of Royal Observatory, Edinburgh, ed. Wolstencroft